RSC Advances

RSC Advances

www.rsc.org/advances

ROYAL SOCIETY
OF CHEMISTRY

www.rsc.org/advances

Journal Name

ARTICLE

Investigation of Photoinduced Electron Transfer on TiO₂ Nanowire Arrays/Porphyrin Composite via Scanning Electrochemical Microscope

Yuan Jiang, Dong-Dong Qin, Yan-Ru Fan, Hui-Xia Guo, Shi-Xia Wang, Xing-Ming Ning, Xiao-Quan Lu*

In the present study, vertically aligned single-crystalline TiO₂ nanowire arrays with various length grown on transparent substrate have been successfully prepared by using a facile hydrothermal method, which were then sensitized with a photoactive compound, 5, 10, 15, 20-tetrakis (4-carboxylphenyl) porphyrin. The material was fully characterized by scanning electron microscope (SEM), X-ray diffraction (XRD) and Ultraviolet-visible absorption spectra (UV-vis). A UV-vis/scanning electrochemical microscope (SECM) platform was developed by utilizing TiO₂ nanowire arrays and the influence of wire length, wavelength of light and light intensity to the electron transfer rate was discussed in detail through measuring probe approach curves. The results have shown that the electron transfer rate in the surface of TiO₂/porphyrin composite was accelerated with increased length of nanowire, probably due to the more porphyrin loading and the appropriate match of conduction band edge of TiO₂ and LUMO energy level of porphyrin molecules, as evidenced by the DFT theoretical calculation. The maximum rate constants of electron transfer was reached at a wavelength of 546 nm and an illumination intensity of 90%. The efficient PET system constructed in this work will, we believe, provide useful information to help people investigate mechanism of charge transfer process in artificial photosysthesis.

Introduction

In the initial steps of photosynthesis, photoinduced electron transfer (PET) is one of the most important process to convert solar energy into chemical energy and have attracted significant scientific attention with the aim to prepare artificial photosynthetic systems, energy harvesting photovoltaic devices and opto-electronic molecular switches.[1-16] The presence of porphyrin in natural photosynthetic systems has ensured the source of electron donor. What's more, porphyrin and its derivatives known as "the pigment of life"[17] are excellent organic semiconductor materials. In this context, many porphyrin and its derivatives linked with acceptor have been designed to emulate photosensitizing, redox-active components, charge separation, the antenna junctions of reaction centers and light harvesting complexes of natural photosynthetic membranes in model studies of artificial photosynthesis.[1,18-23] For all those applications, light-harvesting porphyrin-based supramolecular assemblies is essential for fabrication of supramolecular photo-functional devices.[24-26]

Titanium dioxide (TiO₂) has been studied extensively because of its strong optical absorption, high chemical stability, environmental benignity and low cost.[27] In particularly, TiO₂ nanowire (NW)[28] synthesized by hydrothermal method has become a research hotspot for photoelectrochemical (PEC) conversion due to its large internal surface area, good electrical transport, low charge carrier recombination losses and short diffusion distance for photo-generated carriers in recent years.[29] Many groups have been working on developing TiO₂ NWs in the fields of dye-sensitized solar cells (DSSCs), PEC water oxidation, renewable energy, functional building blocks and photoinduced electron transfer.[30-34] Compared to the formerly used nanoparticles (NPs), NWs as a 1D nanostructure possess the advantages of high length-to-diameter ratio, low number of grain boundaries and surface defects, as well as the rapid electron transport rate along the NW, resulting in high PEC properties achievement.[35] It has been reported that the electron mobility in single crystalline NW was about two orders of magnitude higher than that in NC film.[36,37] A few studies, however, considered the effect of TiO₂ NW length on PET and used TiO₂ nanowire arrays/porphyrin composite as platform to investigate PET process. It is, therefore, of considerable interesting to study the charge transfer process using this novel PET system, in which oriented TiO₂ nanowire arrays grown on transparent substrate as supporting material and porphyin molecules as sensitizer. For this purpose, many optical microscopy techniques, such as fluorescence microscopy and electron microscopy are commonly utilized approaches, which can provide some information to access chemical fluxes from

individual cells.[38] Contrasting with above-mentioned methods, scanning electrochemical microscope (SECM) based on micro- and nano-interface is particularly suitable to determine the kinetics of electron transfer in a wide range of redox-active species with high spatial and architectonics.

A few pioneering work for researching PET process of porphyrin-based system by a new technique of combining SECM and UV-visible light illumination have been reported in our group.[39,40] For example, a electron donor-acceptor linked system of porphyrin as donor and benzoquinone (BQ) as acceptor is developed as sensor platform to detect benzoquinone via PET process. However, this model was not actually efficient to annotate the electron transfer process in photosynthesis and relative kinetic information such as electron transfer rate was not given. To offer deep insight into the mechanism of photosystem, we have constructed here a simple light harvesting model by chemical pathway and investigate the multiple electron-transfer reaction. The relationship between the electron transfer efficiency and length of TiO_2 nanowire was discussed carefully via UV-vis/SECM technique in this study. Additionally, it is found that the charge transfer rate heavily depends on the wavelength of light and light intensity.
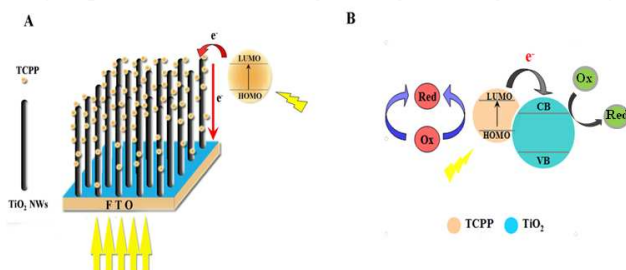
Sche. 1 Schematic illustration of (A) TCPP deposited on TiO_2 NW array electrode, photo-induced charge transfer in the nanocomposite structures. (B) Energy band in the composite structures

Experimental

Reagents

NaCl (AR, Xilong Chemical Ind., Co., Ltd), $K_4Fe(CN)_6$ (AR, Kaixin Chemical Ltd, Tianjin), Tetrabutyl Titanate (TNBT) (AR, Sinopharm Chemical Reagent Co., Ltd, Shanghai) and hydrochloric acid (HCl) (AR, Sigma-Aldrich Trading Co., Ltd, Shanghai) were used as received. 5, 10, 15, 20-tetrakis (4-carboxylphenyl) porphyrin (TCPP) were synthesized by our laboratory as the previous reported methodology. Unless otherwise stated, reagents were of analytical grade and were used as received. All aqueous solutions were prepared by ultrapure water with the resistivity of 18.25 MΩ·cm.

Apparatus

UV-vis spectra measurements were obtained with a UV-1102 spectrometer (Shanghai, China). The morphologies of the TiO_2 nanowire were observed through SEM on ULTRA plus. XRD patterns were recorded using a Shimadzu XD-3A (Japan). TiO_2 sample annealing was conducted in tube furnace of Tianjin Central Experimental Furnace Co., Ltd., model SK-G05123K. Photoelectrochemical (PEC) measurements were performed with a home-built PEC system. A 150 W Xe lamp light resource was used as the irradiation source. PEC measurements were conducted on a CHI900B electrochemical workstation (CH Instruments, Austin, TX). A custom electrolytic cell was made of a Teflon base with cone-shaped lining and a small opening on the back side which was

used for light irradiation. All experiments were carried out at room temperature using a conventional three-electrode, a Pt ultramicroelectrode (UME), a platinum wire and saturated calomel electrode as the working electrode, counter electrode and reference electrode, respectively. A 25 µm diameter Pt UME (RG = 10, RG is the ratio of the overall electrode radius over the platinum disk radius) which sealed into a borosilicate glass capillary under vacuum was used as the SECM tip electrode. The UME was characterized by cyclic voltammetry and optical microscope figure. When a graceful S-model cyclic voltammetry curve (as shown S Fig. 2A) was obtained, it means that the Pt UME is successfully prepared. Fluorine-doped tin oxide (FTO) glasses (with a specific surface conductivity of ca. 10 Ω cm^{-2}) were purchased from Zhuhai Kaivo Electronic Components Co. (Guangdong, China). The FTO glasses were cut into 1×2.5 cm size slides and ultrasonically cleaned in turn in the absolute ethanol, acetone, and deionized water for 10 min, and finally dried with nitrogen gas. EIS experiments were performed on Multi-potentiostat (VMP2, Princeton Applied Research, USA), with a superimposed 5 mV sinusoidal voltage in the frequency range of 10 mHz-100 kHz.

Preparation of TiO_2 NWs and Sensitizer Modification

The preparation of TiO_2 NWs was similar to reference[28] and the detailed procedure was as follows: The mixture of 10 mL deionized water and 5 mL concentrated hydrochloric acid was stirred in a sample vial. After adding 0.5 mL tetrabutyl titanate to the mixture, the reaction mixture was stirred for 15 min. until transparent solution was obtained. Then, one piece of FTO substrate was placed at an angle against the wall of the 25 mL Teflon-liner with the conducing side facing down. The hydrothermal synthesis was proceeded at 180 ℃ for 4, 5, 6, 7, 8, 9 h in a electric oven, respectively. After synthesis, the autoclave was cooled to room temperature in fuming cupboard for half an hour. The TiO_2 films were flushed with deinoized water and ethanol. After annealing at 450 ℃ for 2 h, the TiO_2 films were immersed in 0.1 mM ethanol solution of carboxyl porphyrin for 24 h.[41,42] The prepared TiO_2/porphyrin electrodes were stored in watchglass for use under dark condition.

Photoelectrochemical Behavior

Photoelectrochemical measurements were performed at a UV-vis/SECM platform. SECM experimentation records approach curves where the normalized current $I_T = i_T/i_{T,\infty}$ is plotted versus the normalized distance L = d/a. In the SECM operation, the feedback mode is employed to study the kinetics in order to obtain the kinetics of heterogeneous ET with a good resolution. SECM appratus for photoelectrochemical experiments are described elsewhere. In the experiment, all approach curves are obtained with the same zero origin for a defined sample. I_3^-/I^- in acetonitrile was used as redox couple in this section of experiment.

Theoretical Calculations

The molecular structures of TCPP was optimized with density functional theory (DFT) at the B3LYP/6-31G (d) levels and the HOMO and LUMO energy levels were calculated. All calculations were performed with the Gaussian 03 software package

Results and discussion

Characterization of TiO_2 NWs and TiO_2-TCPP composite The morphologies and thickness of TiO_2 NWs were observed by SEM. Figure 1A presented the top-surface images of a typical synthesized TiO_2 NW array sample. It can be seen that highly uniform and densely packed array of TiO_2 NWs were obtained, with an average wire diameter of approximately 30 nm. The 4.7, 6.3, and

7.2 μm thick TiO_2 nanowire film were achieved after reacting 5 h, 7 h and 8 h, respectively, as shown from cross-sectional view of SEM images in Figure 1B, C and D. Figure 1 clearly indicated that the TiO_2 NWs grown almost perpendicularly against the substrate. The XRD pattern in Figure 2 demonstrated a remarkably dominated (002) peak, suggesting oriented growth of TiO_2 nanowire along [001] direction. The XRD data revealed that the films deposited on FTO substrates are tetragonal rutile TiO_2,[42] which is in good agreement with the published experimental data.[28] In addition, the XRD patterns (Figure 2) indicated the TiO_2 NWs were not only aligned but also were single crystalline along with their length. It is reported that the length of TiO_2 NWs could be varied by changing the growth time.[28] According to this, TiO_2 NWs with different lengths have been fabricated in this work by adjusting the reaction time and the results are listed in the Table 1.
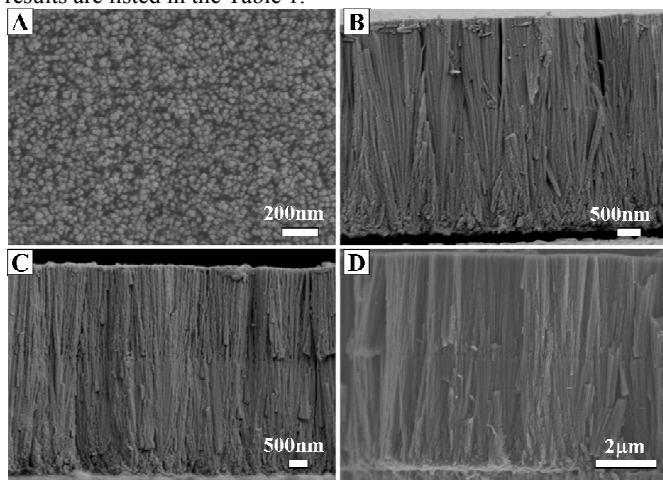
Fig. 1 SEM images of TiO_2 nanowire arrays after two-step growth: (A) top view; (B), (C) and (D) cross-sectional view of samples with the reaction time of 5 , 7 and 8 h, respectively.
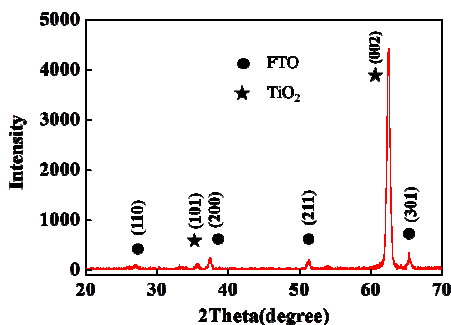
Fig. 2 XRD patterns of TiO_2 film on the FTO substrate prepared by hydrothermal method after annealing at 450 ℃ for 2 h.

TCPP was introduced to the system for efficient absorption of light energy. Carboxylic acid groups are known to be spontaneously adsorbed onto TiO_2 surfaces. They form bidentate chelating, bidentate bridging, and/or ester-like binding with TiO_2 surfaces, which depends on the experimental conditions.[41] The UV-vis absorption spectra of TiO_2 NWs and TiO_2-TCPP nanoposites were shown in Figure 3. TiO_2 NWs displayed a remarkable peak from 350 to 400 nm. The cut off absorption at 400 nm is consistent with typical band gap of rutile TiO_2 (3.0-3.2 eV). TiO_2-TCPP exhibited a typical Soret band at 419 nm and four weak Q-band absorption at 522, 560, 599 and 653 nm, illustrating the successful anchoring of TCPP on to the surface of TiO_2 NWs.
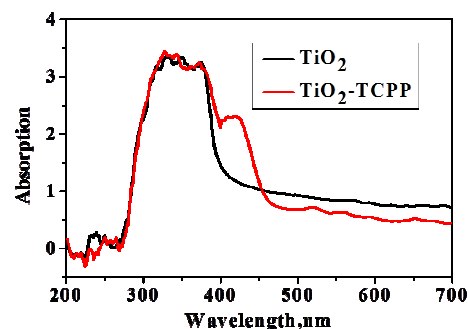
Fig. 3 UV-vis absorption spectra of the TiO_2 NWs (black line) and TiO_2-TCPP (red line).

Effect of the light wavelength and intensity

To examine the effects of light wavelength on the photoelectrochemical response, the PET process of TiO_2-TCPP system was studied under illumination of different wavelength of light with intensity of 100%. In this section of experiment, the I_3^- in acetonitrile was used as sacrificial electron donor. LiI and I_2 were dissolved in the conventional solvent—acetonitrile.[44, 45] Figure 4A shows series of probe approach curves (PACs) at the wavelengths of 469, 487, 515, 531, 546 and 570 nm. As expected, the fit of the experimental probe approach curves to the theoretical ones goes very well and the apparent heterogeneous electron transfer rate constant k_{eff} which is extracted from the fitting of an experimental prove approach curve to the theoretical one is determined according to k_{eff} = $\kappa D/r_T$ in cm s^{-1}. From the fitting, positive feedback has been obtained when the tip approached the TiO_2 NWs due to reaction of I$^-$ with excited TCPP, which indicates that a bimolecular reaction occurs. Porphyrins are able to absorb the certain wavelength of light. Herein, positive feedback was observed when wavelengths of the light are 515, 531, 546 and 570 nm. In contrast, negative feedback was obtained under illumination with wavelength of 469 and 487 nm due to the weak absorption of porphyrin molecules. According to these studies, [46, 47] the most likely charge transfer mechanism is as follows:

$$TiO_2 - TCPP + h\upsilon \rightarrow TiO_2 - TCPP* \qquad (1)$$

$$TiO_2 - TCPP* \rightarrow TiO_2 - TCPP^+ + e_{CB}^-(TiO_2) \qquad (2)$$

$$2TiO_2 - TCPP^+ + 3I^- \rightarrow 2TiO_2 - TCPP + I_3^- \qquad (3)$$

$$I_3^- + 2e^- \rightarrow 3I^- \text{ (at tip electrode)} \qquad (4)$$
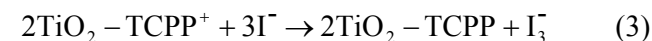
In addition, we also investigated the effect of light intensity on regular probe approach curve. The wavelength of light was fixed while the effect of illumination intensity on k_{eff} was shown in Figure 5. A slowly increasing trend of the current and k_{eff} vs the light intensity was observed when the illumination intensity ranged from 10%-90%. Whereas, both current and k_{eff} decreased once light intensity was increased to 90%. The results demonstrated that light intensity was not the only factor that influenced the k_{eff} and blind strengthening of the illumination intensity was not always working to accelerate electron transfer rate.
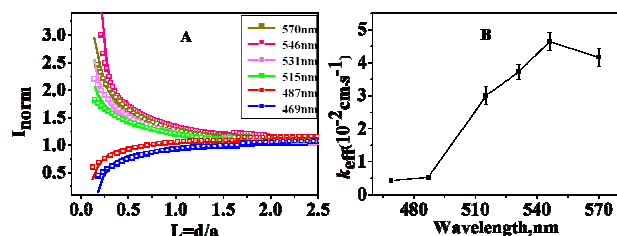
Fig. 4 (A) SECM PACs on an FTO substrate with TiO$_2$ NWs/TCPP film under different light wavelength of illumination (B) Dependence of k_{eff} on the light wavelength with SD definition (n=5).
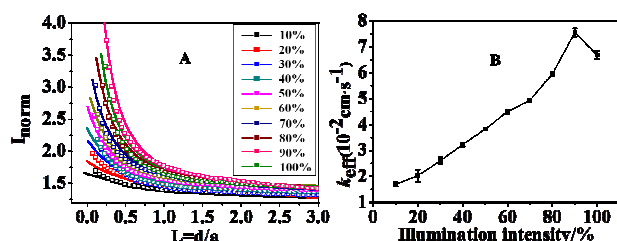
Fig. 5 (A) SECM PACs of FTO substrate developed TiO$_2$ NWs-TCPP under different light intensity at 546 nm (B) Dependence of k_{eff} on the light intensity with SD definition (n=5).

Effect of TiO$_2$ NWs

It is not uncommon that longer TiO$_2$ NW can be obtained by extending the reaction time or repeat growth in fresh precursor solution. But this way would lead to diameter widening of TiO$_2$ NWs and the decrease of surface area due to gap filling caused by following growth. In order to address this issue, NaCl was added in the second or third growth cycle, because it has been reported that Cl$^-$ could selectively adsorb onto the surface of rutile TiO$_2$ nanowire and consequently, leading to wire growth along [001] direction. The results show that the length of TiO$_2$ NWs increased significantly with prolonged reaction time and presence of NaCl but the diameter of wire remained almost unchanged after reported growth (Table 1). This insured an increase in the surface area.[31] On the basis of the above results, we investigated the electron transfer process with different lengths of TiO$_2$ NWs. The wavelength and illumination intensity were fixed. Figure 6 showed length profile of normalized PACs acquired from sample S1-6 in the solution of I$_3^-$/I$^-$ with light wavelength of 546 nm and a intensity of 100%. The PACs of all samples in Figure 6A corresponded to positive feedback, and meanwhile k_{eff} slightly increased with increasing length of wire. We think that the enhanced k_{eff} for longer wire under visible light is likely due to the high loading amount of TCPP on the surface of TiO$_2$ NWs. It has been reported that the porous nanocrystalline TiO$_2$ layer with high surface area serves as an excellent platform for efficient light harvesting.[48,49] In other words, the larger surface area TiO$_2$ NW possesses, the more TCPP anchoring on TiO$_2$ will be.
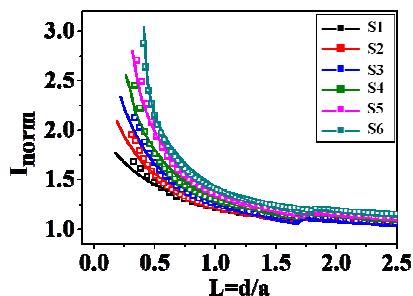
Fig. 6 SECM PACs of TiO$_2$ NWs-TCPP on FTO substrate with different length of TiO$_2$ NWs (S1) 2.5 μm, (S2) 4.7 μm, (S3) 5.3 μm, (S4) 6.3 μm, (S5) 7.2 μm, (S6) 9.2 μm at 546 nm.

Table 1 Electron transfer rate constants (k_{eff}) of TiO$_2$-TCPP with different length of TiO$_2$ nanowires. D is the diffusion coefficient for I$_3^-$ (D =1.37 × 10^{-5} cm·s^{-1}).

Sample	S1	S2	S3	S4	S5	S6
Time(h)	4	5	6	7	8	9
Length(μm)	2.5	4.7	5.3	6.3	7.2	9.2
k$_{eff}$(10^{-2}cm·s^{-1})	2.74	3.288	3.836	4.384	5.151	5.918

Meanwhile, the charge transfer process occurred in TiO$_2$ NWs-TCPP was studied by AC impedance spectroscopy to identify the results obtained from PACs, since electrochemical impedance spectroscopy (EIS) was considered to be a useful tool to characterize the charge-carrier migration.[50] The EIS were measured with the frequency ranging from 100 kHz to 0.01 Hz under illumination. The Nyquist plots for the TiO$_2$ NWs and TiO$_2$ NWs-TCPP electrodes were shown in Figure 7A. Two semicircles at high and medium-frequency ranges as well as a line tilted at an approximately 45° angle to the real axis at low frequency were observed. The equivalent circuit which modelled the TiO$_2$ NWs and TiO$_2$ NWs-TCPP electrode was shown in the lower right of the Figure 7A. In particular, the simulated equivalent circuit consisting of a series of resistance (Rs, starting point of the first semicircile in Nyquist plot, was the ohmic resistance of the electrolyte, membrane and electrode), the resistance of the solid-electrolyte interface layer (R$_{SEI}$, first semicircle in Nyquist plot), charge transfer resistance (R$_{ct}$, second semicircle in Nyquist plot), the constant phase element (CPE) which can replaced the electrochemical double-layer capacitance at the electrode-electrolyte interface, the mass-transfer impedance (Z$_W$, the sloping line in Nyquist plot) which indicated Warburg impedance and represented the diffusion of K$_3$[Fe(CN)$_6$] ions.[51] The reaction between the electrolyte and the surface of the electrode caused the CPE and resistance R$_{SEI}$. Furthermore, the second semicircle was attributed to charge transfer kinetics.[52] In the Nyquist plots, it is observed that the semicircle diameter of TiO$_2$ NWs-TCPP electrode was smaller than that of bare TiO$_2$ NWs electrode, implying that the charge transfer resistance (R$_{ct}$) of TiO$_2$ NWs-TCPP is smaller than that of TiO$_2$ NWs. As depicted in Table S1, R$_{ct}$ reduced in turn for the sample of S1 to S6. These results revealed that the charge transfer rate in TiO$_2$ NWs-TCPP was higher than TiO$_2$ NWs, and S6 was higher than that for S5, S4, S3, S2 and S1, consistent with the results gained from PACs.
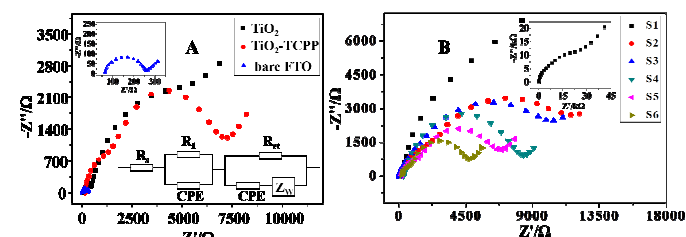
Fig. 7 (A) Typical EIS, presented as Nyquist plots for the TiO_2 and TiO_2-TCPP electrodes under 546 light illumination and the equivalent circuit used to fit the EIS. (B) Typical EIS, presented as Nyquist plots for varying length of TiO_2-TCPP electrodes under 546 light illumination.

Theoretical Calculations

In order to testify the electron transfer pathway, we have performed density functional theory (DFT) calculations at the B3LYP/6-31G level to gain further insight into the geometries and electronic properties of TCPP. Six typical orbitals of TCPP have been exhibited as follows: HOMO-2, HOMO-1, HOMO, LUMO, LUMO+1 and LUMO+2, their values were -6.63, -5.76, -5.38, -2.74, -2.73 and -1.85 eV, respectively. All unoccupied orbital values are higher than the lower bound level of the conduction band (CB) of TiO_2, indicating that the efficiency of charge injection from the excited sensitizer molecule to the TiO_2 CB is viable.[53]

Transfer of electrons from the singlet excited-state of TCPP to the TiO_2 NWs must be downhill in energy. In this measurement, if the singlet excited-state of TCPP is more positive than that of the CB of TiO_2 NWs, then electrons should transfer easily from TCPP into TiO_2. As shown in Scheme 2, photoexcitation of TCPP can give rise to electrons transferring from the HOMO to the LUMO. Afterwards, since the CB edge of TiO_2 is well matched with energy level of the LUMO of TCPP and electronic coupling between the TCPP and the TiO_2 surface through the carboxyl group is fairly strong, efficient electron injection from the TCPP singlet excited-state to the CB of TiO_2 occurs. Meanwhile, dye regeneration reaction happens via direct electron transfer from I^- to the HOMO of TCPP.
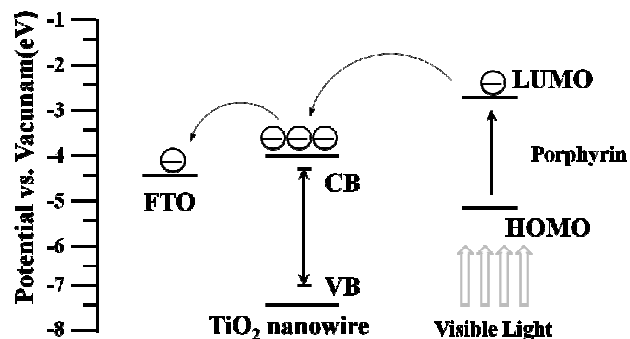
Sche. 2 Schematic Energy Level Diagram and Electron Transfer Path.

Conclusions

In summary, A photo-induced electron transfer (PET) system was constructed by combination of vertically aligned single crystal TiO_2 nanowire arrays and porphyrin to investigate the mechanism of charge transfer process in artificial photosythesis. The reaction mechanism of PET process was proposed and the important kinetic information was evaluated by using electrochemical impedance spectra and a unique technique of UV-vis/Scanning Electrochemical Microscope(SECM). It is found that the electron transfer rate was significantly accelerated once longer nanowire arrays was used due to more porphyrin loading and the appropriate match of conduction band edge of TiO_2 and LUMO energy level of porphyrin molecules, as evidenced by DFT calculation. It is found that the rate constants of electron transfer reach the maximum at a wavelength of 546 nm and an illumination intensity of 90%. In a word, our results show that the integrated system in this work is an effective platform for deep insight into the mechanism of PET process, which is known as critical part of the artificial photosynthesis.

Notes and references

[a] Key Laboratory of Bioelectrochemistry & Environmental Analysis of Gansu Province, College of Chemistry & Chemical Engineering, Northwest Normal University, 730070, China; E-mail: taaluxq@gmail.com

∗ Corresponding author

1 M.R. Wasielewski,. *Chem. Rev* 1992, 92, 435.

2 M.P. Debreczeny, W.A. Svec, Wasielewski, M. R. *Science* 1996, 274, 584.

3 S. Wallin, C. Monnereau, E. Blart, J.R. Gankou, F. Odobel, L. Hammarstrom, *J. Phys. Chem. A* 2010, 114, 1709.

4 M. Berberich, A.M. Krause, M. Orlandi, F. Scandola, F. Wurthner, *Angew. Chem* 2008, 120, 6718.

5 H. Imahori, S. Fukuzumi, *Adv. Funct. Mater* 2004, 14, 525.

6 U. Bach, D. Lupo, P. Comte, J.E. Moser, F. Werssortel, J. Salbeck, H. Spreitzer, M. Gratzel, *Nature* 1998, 395, 583.

7 M. Gratzel, *Nature* 2001, 414, 338.

8 A. Hagfeldt, M. Gratzel, *Acc. Chem. Res* 2000, 33, 269.

9 N. Aratani, D. Kim, A. Osuka, *Acc. Chem. Res* 2009, 42, 1922.

10 A. Uetomio, M. Kzaki, S. Suzuki, K.I. Yamanaka, O. Ito, K. Okada, *J. Am. Chem. Soc* 2011, 133, 13276.

11 V. Garg, G. Kodis, P.A. Liddell, Y. Terazono, T.A. Moore, A.L. Moore, D. Gust, *J. Phys. Chem. B* 2013, 117, 11299.

12 Y. Leroux, D. Schaming, L. Ruhlmann, P. Hapiot, *Langmuir* 2010, 26, 14983.

13 Y. Terazono, G. Kodis, K. Bhushan, J. Zaks, C. Madden, A.L. Moore, T.A. Moore, G.R. Fleming, D. Gust, *J. Am. Chem. Soc* 2011, 133, 2916.

14 M. Gratzel, *Inorg. Chem* 2005, 44, 6841.

15 Y.Y. Liang, Y. Wu, D.Q. Feng, S.T. Tsai, H.J. Son, G. Li, L.P. Yu, *J. Am. Chem. Soc* 2009, 131, 56.

16 K.S. Leschkies, R. Divakar, J. Basu, E.E. Pommer, J.E. Boercker, C.B. Carter, U.R. Kortshagen, D.J. Norris, E.S. Aydil, *Nano. Lett* 2007, 7, 1793.

17 P.D. Frischmann, K. Mahata, F. Wurthner, *Chem. Soc. Rev* 2013, 42, 1847.

18 M.R. Wasielewski, *Acc. Chem. Res* 2009, 42, 1910.

19 (a) H. Imahori, K. Tamaki, D.M. Guldi, C. Luo, M. Fujitsuka, O. Ito, Y. Sakata, S. Fukuzumi, *J. Am. Chem. Soc* 2001, 123, 2607. (b) H. Imahori, D.M. Guldi, K. Tamaki, Y. Yoshida, C. Luo, Y. Sakata, S. Fukuzumi, *J. Am. Chem. Soc* 2001, 123, 6617. (c) F. Spanig, M. Ruppert, J. Dannhauser, A. Hirsch, D.M. Guldi, *J. Am. Chem. Soc* 2009, 131, 9378. (d) F.D. Souza, N.K. Subbaiyan, Y.S. Xie, J.P. Hill, K. Ariga, K. Ohkubo, S. Fukuzumi, *J. Am. Chem. Soc* 2009, 131, 16138.

20 (a) F. Wessendorf, J.F. Gnichwitz, G.H. Sarova, K. Hager, U. Hartnage, D.M. Guldi, A. Hirsch, *J. Am. Chem. Soc* 2007, 129, 16057. (b) H.

Lemmetyinen, N.V. Tkachenko, A. Efimov, M. Niemi, *J. Phys. Chem. C* 2009, 113, 11475.

21 (a) H. Imahori, *J. Phys. Chem. B* 2004, 108, 6130. (b) F.D. Souza, E. Maligaspe, K. Ohkubo, M.E. Zandler, N.K. Subbaiyan, S. Fukuzumi, *J. Am. Chem. Soc* 2009, 131, 8787.

22 J.H. Kim, M. Lee, J.S. Lee, C.B. Park, *Angew. Chem. Int. Ed* 2012, 51, 517.

23 P.D. Frischmann, K. Mahata, F. Wurthner, *Chem. Soc. Rev* 2013, 42, 1847.

24 T. Honda, T. Nakanishi, K. Ohkubo, T. Kojima, S. Fukuzumi, *J. Am. Chem. Soc* 2010, 132, 10155.

25 C.B. KC, K. Stranius, P. D'Souza, N.K. Subbaiyan, H. Lemmetyinen, N.V. Tkachenko, F. D'Souza, *J. Phys. Chem. C* 2013, 117, 763.

26 D. Bonifazi, O. Enger, F. Diederich, *Chem. Soc. Re* 2007, 36, 390.

27 M. Xu, P.M. Da, H.Y. Wu, D.Y. Zhao, G.F. Zheng, *Nano. Lett* 2012, 12, 1503.

28 B. Liu, E.S. Aydil, *J. Am. Chem. Soc* 2009, 131, 3985.

29 K. Shankar, J.I. Basham, N.K. Allam, O.K. Varghese, G.K. Mor, X.J. Feng, M. Paulose, J.A. Seabold, K.S. Choi, C.A. Grimes, *J. Phys. Chem. C* 2009, 113, 6327.

30 C.Y. Zha, L.M. Shen, X.Y. Zhang, Y.F. Wang, B.A. Korgel, A. Gupta, N.Z. Bao, *Appl. Mater. Interfaces* 2014, 6, 112.

31 Z.J. Zhou, J.Q. Fan, X. Wang, W.H. Zhou, Z.L. Du, S.X. Wu, *Appl. Mater. Interfaces* 2011, 3, 4349.

32 (a) F.M. Pesci, G.M. Wang, D.R. Klug, Y. Li, A.J. Cowan, *J. Phys. Chem. C* 2013, 117, 25837. (b) Y.C. Pu, Y.C. Ling, K.D. Chang, C.M. Liu, J.Z. Zhang, Y.J. Hsu, Y. Li, *J. Phys. Chem. C* 2014, 118, 15086.

33 I.S. Cho, M. Logar, C.H. Lee, F.B. Prinz, X.L. Zheng, *Nano. Lett* 2014, 14, 24.

34 A. Wolcott, W.A. Smith, T.R. Kuykendall, Y.P. Zhao, J.Z. Zhang, *Small* 2009, 5, 104.

35 H. Wang, Y.S. Bai, H. Zhang, Z.H. Zhang, J.H. Li, L. Guo, *J. Phys. Chem. C* 2010, 114, 16451.

36 L. Forro, O. Chauvet, D. Emin, L. Zuppiroli, H. Berger, F. Levy, *J. Appl. Phys* 1994, 75, 633.

37 M. Law, L.E. Greene, J.C. Johnson, R. Saykally, P.D. Yang, *Nature. Materials* 2005, 4, 455.

38 K. Mckelvey, S. Martin, C. Robinson, P.R. Unwin, *J. Phys. Chem. B* 2013, 117, 7878.

39 X.Q. Lu, Y.Q. Hu, W.T. Wang, J. Du, H.X. He, R.X. Ai, X.H. Liu, *Colloid. Surface. B* 2012, 103, 608.

40 W.T. Wang, Y.Q. Hu, C.M. Wang, X.Q. Lu, *Eletrochimica. Acta* 2012, 65, 244.

41 S. Eu, S. Hayashi, T. Umeyama, Y. Matano, Y. Araki, H. Imahori, *J. Phys. Chem. C* 2008, 112, 4396.

42 S. Hayashi, M. Tanaka, H. Hayashi, S. Eu, T. Umeyama, Y. Matano, Y. Araki, H. Imahori, *J. Phys. Chem. C* 2008, 112, 15576.

43 (a) X.J. Feng, K. Shankar, M. Paulose, C.A. Grimes, *Angew. Chem* 2009, 121, 8239. (b) J.M. Wu, H.C. Shih, W.W. Wu, *Nanotechnology* 2006, 17, 105. (c) E.E. Pommer, B. Liu, E.S. Aydil, *Phys. Chem. Chem. Phys* 2009, 11, 9648. (d) A. Kumar, A.R. Madaria, C.W. Zhou, *J. Phys. Chem. C* 2010, 114, 7787.

44 K. Hosomizu, H. Imahori, U. Hahn, J.F. Nierengarten, A. Listorti, N. Armaroli, T. Nemoto, S. Isoda, *J. Phys. Chem. C* 2007, 111, 2777.

45 Y. Shen, K. Nonomura, D. Schlettwein, C. Zhao, G. Wittstock, *Chem. Eur. J* 2006, 12, 5832.

46 U.M. Tafashe, K. Nonomura, N. Vlachpoulos, A. Hagfeldt, G. Wittstock, *J. Phys. Chem. C* 2012, 116, 4316.

47 J.S. Lee, K.H. You, C.B. Park, *Adv. Mater* 2012, 24, 1084.

48 J.R. Jennings, A. Ghicov, L.M. Peter, P. Schmuki, A.B. Walker, *J. Am. Chem. Soc* 2008, 130, 13364.

49 E. Galoppini, J. Rochford, H.H. Chen, G. Saraf, Y.C. Lu, A. Hagfeldt, G. Boschloo, *J. Phys. Chem. B* 2006, 110, 16159.

50 (a) P. Diao, Z.F. Liu, *J. Phys. Chem. B* 2005, 109, 20906. (b) X. Pan, Y. Zhao, S. Liu, C.L. Korzeniewski, S. Wang, Z.Y. Fan, *Appl. Mater. Inter* 2012, 4, 3944.

51 Y.H. Jang, X.K. Xin, M. Byun, Y.J. Jiang, Z.Q. Liu, D.H. Kim, *Nano. Lett* 2012, 12, 479.

52 M.M. Rahman, J.Z. Wang, D. Wexler, Y.Y. Zhang, X.J. Li, S.L. Chou, H.K.J. Liu, *Solid. State. Electrochem* 2010, 14, 571.

53 S. Karthikeyan, J.Y. Lee, *J. Phys. Chem. A* 2013, 117, 10973.